英文摘要

The objective of this research project (term of execution, 17 months) is to develop a microscope based on infrared-visible sum-frequency generation (SFG) for applications to surface catalytic reactions and biologically relevant surfaces. Originally the project was until July 31, 2009. However it was extended to December 31, because, unexpectedly, the laboratory to which the procured optical table was supposed to be installed had not been available until then.

First the sample part of the SFG microscope has been constructed. A breadboard is used to mount optical components in a vertical plane. He-Ne laser outputs are used as a guide to align those optical components. The incident angles of the mid-infrared and 532 nm beams are chosen as 70º and 60º, respectively. To fulfill the phase matching condition, the angle of the SFG output is estimated to be 61.2º, which lies in between the mid-infrared and visible beams. Since a broadband femtosecond infrared light (about 400 cm^{-1} width) will be used in order to achieve multiplex SFG measurements, variation in the angle of the SFG output with the frequency of the infrared light is also calculated. We are currently making an effort to develop an SFG microscope by integrating the sample part into an existing femtosecond laser system.

While waiting for the optical table to be installed, we have made full use of the procured CCD detector and combined it with a laboratory-designed Raman microscope. By using this apparatus, we study biofilms consisting of *Escherichia coli* grown on a glass substrate. A biofilm is a complex community of microorganisms that reside in a film-like architecture of extracellular polymeric substances. Comprehensive molecular vibrational imaging has been successfully demonstrated for the first time, which unravels highly heterogeneous nature of the *E. coli* biofilm. SFG studies of those biofilms are planned in the near future.

英文關鍵詞

Sum-frequency generation (SFG), optical microspectroscopy, molecular vibrational imaging, biofilms

中文摘要

此研究計畫的目的(執行期間爲 17 個月)爲要發展 infrared-visible sum-frequency generation (SFG) 顯微術應用在表面催化反應及和生物體表面。原本此計畫期限是至 2009 年 7 月 31 日，而後延長至 12 月 31 日。延長的原因在於爲進行此計畫而購買的光學桌無法在計畫截止前完成安裝測試，故延長至 2009 年年底。

首先 SFG 顯微鏡中放置樣品的元件已經架設完成，使用另一個光學元件架設平台在垂直的平面上。輸出氦-氖雷射來引導以便校準光學元件。中紅外光與波長 532 nm 的雷射光的入射角分別選定爲 70 度和 60 度。滿足實驗的條件下，可以使 SFG 訊號輸出落在中紅外光與可見光區，此時 SFG 輸出訊號的角度大約 61.2 度。爲了達到 multiplex SFG 的量測，我們使用寬波帶的飛秒紅外線光（波寬大約 100 cm^{-1}），也同時計算紅外線光頻率在 SFG 訊號輸出上的角度變化。目前我們正致力於將現有的雷射系統與樣品作結合發展出 SFG 顯微術。

等待光學桌安裝的同時，我們充分利用已購買的 CCD 偵測器與實驗室的拉曼顯微鏡結合。使用這些器材，我們可以研究培養在玻璃基質上由大腸桿菌所組成的生物薄膜。生物薄膜是一種複雜的微生物共同體，它存在於長的像薄膜結構的胞外聚合物質。我們首當先例成功得到大腸桿菌分子振動的影像，這將會高度顯現大腸桿菌的表面異質特性。在不久的將來，我們計畫將 SFG 應用在這些生物薄膜的研究上。

中文關鍵詞

合頻波、顯微光譜術、分子成像、生物薄膜、表面催化反應

目錄

1. Introduction

Surfaces are ubiquitous in chemical processes. They play a central role in solvent extraction, catalytic reactions, biochemical reactions in cells, and so on. However, compared to the long history of studies on the bulk, only little has been understood about surfaces from a molecular viewpoint. We know far less about dynamical information on molecules or ions involved in surface catalytic reactions and in biologically relevant surfaces such as membranes and biofilms.

IR–visible sum-frequency generation (SFG) spectroscopy, initiated by Shen et al.[1] in 1987, is a powerful technique to measure vibrational spectra at surfaces/interfaces. Because this technique is based on a second-order nonlinear optical process,[2,3] the vibrational information contained is inherently interface-specific. SFG spectroscopy has found many applications in various disciplines of surface science including basic air–liquid interfaces,[4,5] self-assembled monolayers (SAMs),[6–8] adsorbed species at a solid–liquid interface,[6] clean surfaces under ultra-high vacuum.[9] Unfortunately, however, vibrational spectra obtained with SFG spectroscopy are spatially averaged, and hence detailed vibrational information on chemical heterogeneity at interfaces is lost in many cases. To facilitate space-resolved SFG measurements toward molecular vibrational imaging of surfaces, much effort has recently been devoted to combine SFG spectroscopy with either near-field[10,11] or far-field[12–14] microscope.

Saykally et al.[10] used near-field scanning optical microscopy (NSOM) combined with SFG. Their light source was a Ti:sapphire laser/amplifier system operated at 1 kHz and an optical parametric amplifier (OPA). An 800 nm pulse (80 fs, ~3 μJ) and a mid-IR pulse (2.8–10 μm, 155 fs, ~10 μJ) were incident upon the sample in collection mode. The spatial resolution of ~108 nm was achieved. They demonstrated SFG NSOM for chemical vapor deposited (CVD) disk of ZnSe, with data acquisition time of 30–35 min for 200 × 200 pixel arrays. Another near-field SFG imaging has been done by Y. Shen et al.[11] They used a Q-switched Nd:YLF laser as a light source. The fundamental (1047 nm) and second harmonic (523.5 nm) were combined to illuminate the sample that was mounted with an index-matching oil on a fused silica prism under total internal reflection. The SFG signal was collected by an Al-coated fiber probe. They applied their SFG microscope to organic nanocrystals, showing that the spatial resolution of ~360 nm was achieved. However, it should be noted that the SFG microscope developed by Shen et al. uses near-IR light in the SFG process instead of mid-IR light, which results in poorer molecular specificity.

Far-field SFG microscopy is advantageous in that it does not require scanning and nanoscopic tip (near-field fiber probe) which collects SF waves, but the signal is expected to

be much weaker than in near-field SFG microscopy. Kuhnke et al.[12] developed an IR–visible far-field SFG microscope using a diffraction grating. With this method, they succeeded in acquiring direct SFG images without scanning. The laser source used was a Nd:YAG laser with 35 ps pulse duration and 20 Hz repetition rate. A 532 nm pulse and mid-IR pulse derived from an OPA were focused onto the sample with ordinary SFG geometry. A pair of camera lenses focused an intermediate image of the illuminated sample region on the grating. The SFG signal reflected by the grating was then collected with an objective and refocused with a tube lens onto a charge-coupled device (CCD) camera. They estimated the spatial resolution to be 4.9 μm in horizontal and 3.1 μm in vertical direction, which are worse than those achieved with the NSOM method. They used as a demonstration SAMs of the alkanethiol CH_3–$(CH_2)_{17}$–SH. Baldelli et al.[14] also developed this type of SFG imaging microscope and demonstrated it for microcontact-printed SAMs. Despite these pioneering work, development of SFG imaging microscopy and its application to surface science is still a challenging topic.

In this grant proposal, we aimed at developing a new SFG imaging microscope system that is applicable to tracing dynamical behavior of surface catalytic reactions. We planned to use a 1-kHz repetition-rate femtosecond Ti:sapphire laser/amplifier and OPA system as a light source. An image of the target surface is directly acquired by a CCD camera in combination with a diffraction grating, which is similar to the previous setup.[12,14] The spatial resolution is in principle determined by the wavelength of the visible light, not by that of the mid-IR light. The time resolution of sub-picosecond to picosecond[15–18] is anticipated, which enables one to monitor ultrafast phenomena at surfaces. Wavelength tunability of the incident visible beam offers new possibilities of using electronic resonance enhancement in the SFG process.

However in the course of the project, we found that the optical table which we procured could not be installed until the late stage of the project due to a serious delay in construction of the university facility. Therefore we had to apply for five-month extension of the project. Meanwhile we first built up the sample part of the SFG imaging microscope. The optimum angle of the SFG output was calculated for given angles of incoming visible and IR beams on the basis of the standard theory of SFG.[3] The optical components were aligned on a breadboard so that the three beams (the visible and IR inputs, and the SFG output) satisfy the phase matching condition and achieve high SFG efficiency.

Furthermore, while waiting for the optical table to be installed, we made full use of the procured CCD detector and combined it with a laboratory-designed Raman microscope. Raman microspectroscopy is capable of molecular vibrational imaging, the concept of which is analogous to SFG imaging, although it is intrinsically nonspecific to surfaces/interfaces. We used this technique to study biofilms.[19–21] A biofilm is defined as a microbial community

encapsulated in a self-produced extracellular polymeric substances (EPS) adherent to a living or inert surface.[21] Biofilms have been chosen to study in this project mainly because they involve biologically relevant surfaces, which too are a target of this project.

Biofilms are found everywhere; they can grow on a tooth, on the surface of a pipe, in a catheter, and so on. They exhibit high antibiotic resistance compared with a planktonic counterpart.[20] Different microcolonies in a biofilm are known to communicate with one another, and this phenomenon is called quorum sensing.[22] Despite those intriguing characteristics and their broad importance in science, the structure and functions of biofilms have not been understood at the molecular level.[23–28] In this work, Raman microspectroscopy is used (i) to analyze biofilms extracted from activated sludge that is used in waste-water treatment and (ii) to understand more fundamental properties of biofilms by using a model system that consists of *Escherichia coli*. The former will demonstrate the potential of Raman microspectroscopy for *in situ* biofilm analysis, while the latter is expected to serve as a good starting point of more systematic studies of the structure and functions of biofilms. A Raman mapping experiment has revealed highly heterogeneous molecular distribution associated with biofilm formation. In this regard, SFG studies of biofilms, which allow for IR imaging with sub-μm spatial resolution, will also be very interesting.

2. Methods

2.1. SFG microspectrometer

The SFG part of the microspectrometer is the same as the standard configuration in the second-generation (multiplex) SFG spectrometer.[29,30] The principle of multiplex SFG spectroscopy is depicted in Fig. 1. The target surface is irradiated with a broadband IR pulse and a narrowband visible pulse (wavelength = 532 nm), and the SFG signal is generated in the

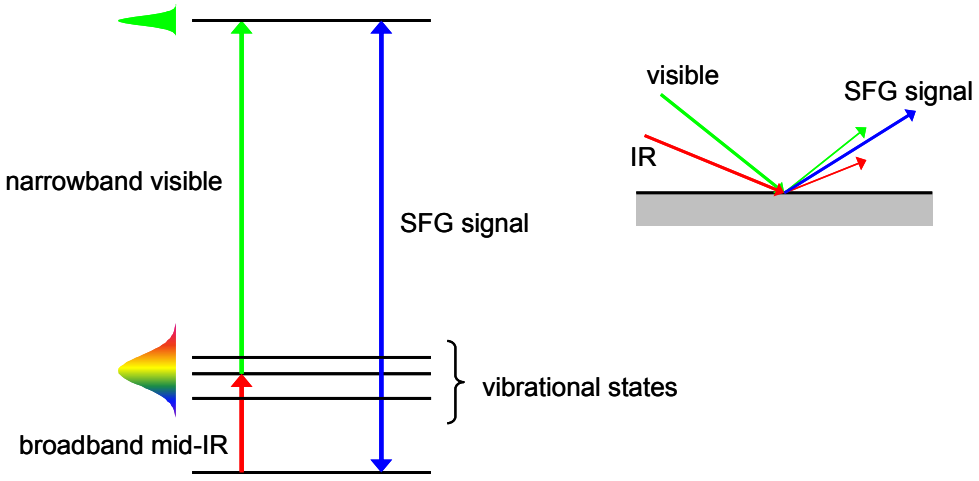

Fig. 1. Principle of IR–visible sum-frequency generation (SFG) process.

phase-matched direction. To fulfill the phase-matching condition and get a sufficient SFG signal, both the visible and mid-IR pulses are incident upon the surface with angle of 60 to 70 degrees from the surface normal. The broadband IR pulse generates a vibrational spectrum over 400 cm^{-1} range.

The most significant part of the apparatus lies in the imaging part. An SFG signal cannot be generated efficiently with ordinary forward or epi-detection configuration, where both visible and IR beams are incident perpendicular to the sample surface. In this proposal, we use a pair of camera lenses to focus an intermediate 1:1 image of the irradiated surface area on a diffraction blazed grating (see Fig. 2). The SFG signal reflected by the grating is then collected with a 10× long-working distance microscope objective and refocused with a tube lens onto a CCD camera with 1024 × 1024 pixels of $(13\ \mu m)^2$ area each. Reflected visible and IR beams are blocked by a shortpass filter. The SFG image for a selected vibrational band within the broadband IR is obtained using a bandpass filter with very small bandwidth. Another bandpass filter is used when we measure the "background image" that contains only vibrationally nonresonant signal. Subtraction of these two images yields the SFG image that has higher vibrational contrast. Depending upon the objective used, a resolution down to 1 μm can be expected. With a magnification factor of 10, the total field of view seen by the CCD is ~$(500\ \mu m)^2$, which should be large enough for many of surface studies.

2.2. Confocal Raman microspectrometer

A schematic layout of our confocal Raman microspectrometer is shown in Fig. 3. It consists of a He-Ne laser (wavelength = 632.8 nm), a custom-made microscope, an imaging

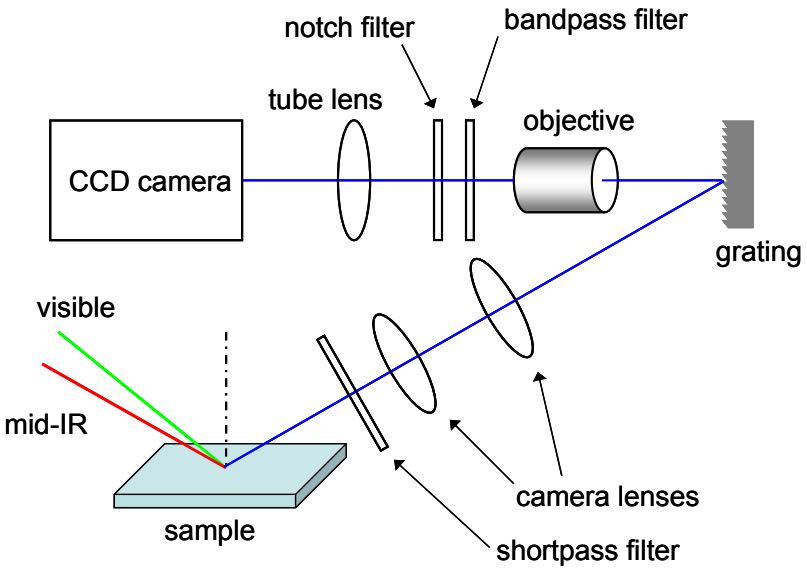

Fig. 2. Optical layout of the SFG imaging microscope.

spectrograph, and a CCD detector, which was originally purchased for the SFG experiment. The excitation laser is focused onto the sample set on the microscope stage by a 100× objective, and the back-scattered Raman signal is collected by the same objective. A pinhole (diameter = 50 μm) is located in front of the spectrograph to achieve confocal detection. When an XYZ piezoelectric translation stage is implemented, the apparatus is capable of doing Raman mapping. The estimated spatial resolution is 300 nm in the lateral direction and 3.1 μm in the axial (depth) direction.

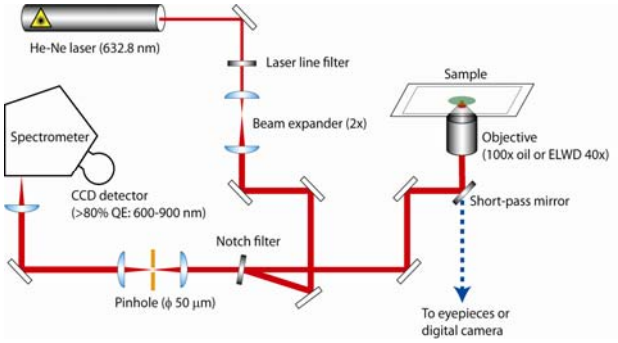

Fig. 3. Schematic diagram of the confocal Raman microspectrometer.

3. Results and discussion

3.1. Development of the sample part

We have constructed the sample part of the SFG imaging microscope (Fig. 4). This part is the key to determine high generation efficiency of the SFG signal. Since SFG is a parametric process, energy conservation must be fulfilled:

$$\omega_{\mathrm{Vis}} + \omega_{\mathrm{IR}} = \omega_{\mathrm{SFG}} . \qquad (1)$$

Here ω_{Vis}, ω_{IR}, and ω_{SFG} are the angular frequencies of the incident visible light, the incident IR light, and the SFG signal, respectively. In addition to Eq. (1), momentum conservation is required as well:

Fig. 4. Sample part of the SFG setup.

$$\boldsymbol{k}_{\mathrm{Vis}} + \boldsymbol{k}_{\mathrm{IR}} = \boldsymbol{k}_{\mathrm{SFG}} , \qquad (2)$$

where $\boldsymbol{k}_{\mathrm{Vis}}$, $\boldsymbol{k}_{\mathrm{IR}}$, and $\boldsymbol{k}_{\mathrm{SFG}}$ are the wave vectors of the incident visible light, the incident IR light, and the SFG signal, respectively. Equation (2) is known as the phase matching condition.[2,3] For an SFG process shown in Fig. 5, Eq. (2) can be written as

$$\omega_{\mathrm{Vis}} \sin\theta_{\mathrm{Vis}} + \omega_{\mathrm{IR}} \sin\theta_{\mathrm{IR}} = \omega_{\mathrm{SFG}} \sin\theta_{\mathrm{SFG}} , \qquad (3)$$

where θ_{Vis}, θ_{IR}, and θ_{SFG} denote the angles with respect to the surface normal, of the incoming visible light, the incoming IR light, and the SFG signal, respectively. The optical components that introduce the visible and IR inputs and collect the SFG output must be aligned so as to satisfy Eq. (3); otherwise the SF signal will not be generated efficiently. Here the incident angles of the visible (532 nm) and mid-IR (3000 cm^{-1}) beams are chosen as 60º and 70º, respectively. The angle θ_{SFG} that satisfies Eq. (3) is calculated to be 61.2º, which lies in

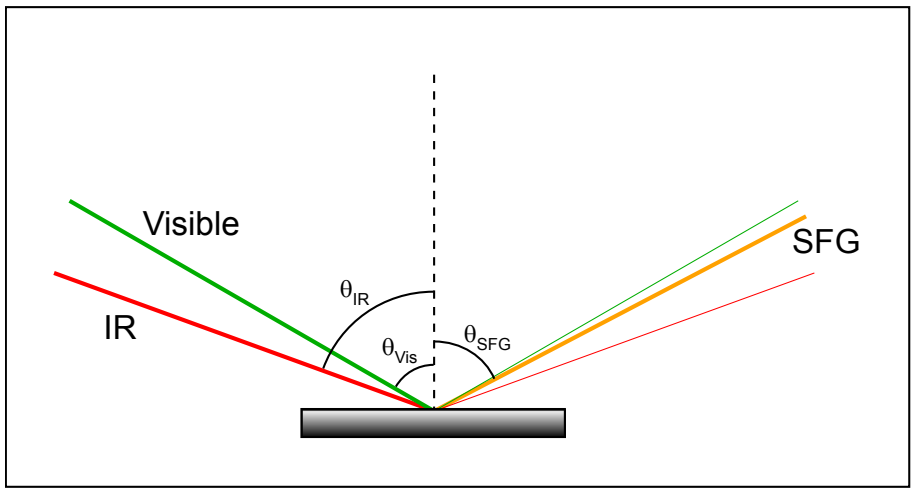

Fig. 5. SFG process at a surface (see text for details).

between the IR and visible beams. The two camera lenses (see Fig. 2) need to be put along this direction.

A broadband IR light will be used, so ω_{IR} changes within the band width (~400 cm^{-1}). We also take into account this variation in ω_{IR}. Given that the band center of the IR radiation is 3000 cm^{-1}, the corresponding wavelength changes from 3.125 to 3.571 μm. Again by using Eq. (3), the angle θ_{SFG} is found to change from 61.1º to 61.3º accordingly, which is negligibly small compared to the high f-number of the camera lenses used.

3.2. Molecular vibrational imaging of biofilms

(a) Biofilms extracted from activated sludge

Two types of activated sludge-extracted biofilms have been provided by our collaborator at Tsukuba University. They are denoted biofilms 1 and 2 (see Fig. 6).

Fig. 6. Biofilms 1 and 2.

Figure 7 shows two representative space-resolved Raman spectra measured from biofim 1. Inspection at various locations on biofilm 1 shows that Raman spectra of biofilm 1, except feature-less spectra due to autofluorescence, fall into those two categories. The spectrum in Fig. 7a shows characteristic features of carotenoids. The prominent bands centered at 1514, 1159, and 1010 cm^{-1} are assigned to the C=C stretch, the C–C stretch, and the CH_3 rock, respectively.[31] Therefore this Raman spectrum strongly suggests the presence of abundant carotenoids in biofilm 1. In contrast to the Raman spectrum in Fig. 7a, that in Fig. 7b is dominated by a sharp, intense band that appears at 996 cm^{-1}. Based on the fact that Raman bands originating from abundant CH groups in biological samples, such as the CH bend, are not clearly observed in this spectrum and that the Raman shift of 996 cm^{-1} is close to the SO_4^{2-}

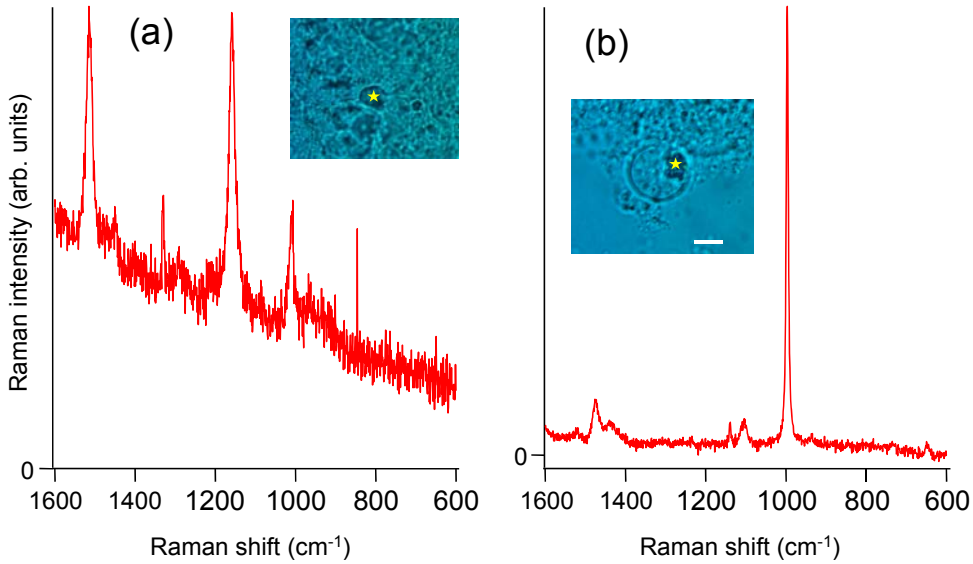

Fig. 7. Two representative space-resolved Raman spectra measured from biofilm 1 together with optical micrographs. The bar in the optical micrograph in (b) measures 5 μm.

symmetric stretch frequency, some inorganic compounds[23] (minerals) are likely to exist in biofilm 1.

In contrast with white, film-like biofilm 1, biofilm 2 is a dark-green suspension. Under the microscope, biofilm 2 does exhibit a substantially different world from biofilm 1. Figure 8 shows an optical microscope image of biofilm 2, which captures a distinctive helical structure extending more than 100 μm. This structure turns out to be the cyanobacteria called Spirulina (*A. platensis*). The space-resolved Raman spectrum obtained at a position on the helix is also displayed in Fig. 8. The Raman spectrum looks very complicated. Assignment of those Raman bands to common biological molecules (nucleic acids, proteins, and polysaccharides) available in reference database[32,33] has been attempted but, so far, in vain. A clue to solve this conundrum would be that unlike ordinary Raman bands of biological samples, most of the

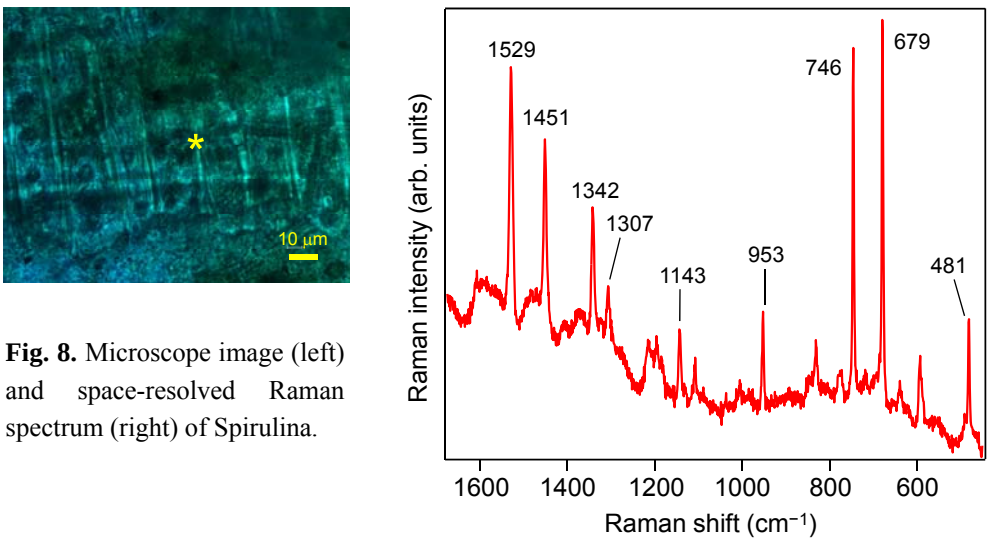

Fig. 8. Microscope image (left) and space-resolved Raman spectrum (right) of Spirulina.

Raman bands observed are extremely sharp. Substances responsible for those bands may occur in crystals.

In conclusion, Raman microspectroscopy has been demonstrated to be highly suitable for *in situ* studies of biofilms used as a bioremediation tool, despite their complicated nature.

(b) Escherichia coli biofilm

In order to understand the structure and functions of biofilms from a more fundamental aspect, a model system for biofilms needs to be investigated. Although the biofilms that are used practically in waste-water treatment are interesting to study, they are simply too complex, as shown above, to perform a systematic study. In this study, a biofilm of well-known Gram-negative bacteria *E. coli* is used. Since *E. coli* is widely used in microbiology and biotechnology as a model microorganism, Raman studies of an *E. coli* biofilm will serve as an excellent platform for *in vivo* characterization of biofilms at the molecular level.

Space-resolved Raman spectra of an *E. coli* biofilm 24 hours after initiating cell culture are shown in Fig. 9. Even at this early stage of growth, the biofilm was heterogeneous; a dense region (the upper photograph) and a less dense region (the lower photograph) were found. However the Raman spectra measured in those two regions look nearly identical. Both spectra agree quite well with the Raman spectrum of planktonic *E. coli* reported previously.[34] It is thus concluded that the biofilm shown in Fig. 9 is in the first stage of growth, where initial adhesion of planktonic cells to the substrate takes place.[20] After one week, as can be seen from the optical micrographs in Fig. 10, the biofilm became much more heterogeneous; a number of island-like structures ("microcolonies") formed. The Raman spectra measured outside the microcolony (spectrum C) is similar to what we observe from a planktonic cell. The Raman spectra measured inside the microcolony (spectra A and B) show many additional bands compared to spectrum C. Some of those Raman bands are identified as the CH bend of aliphatic chains (1455 cm^{-1}), the COO^- symmetric stretch (1408 cm^{-1}), the breathing mode of phenylalanine residues in the side chains (1005 cm^{-1}), and the Fermi doublet[35] of a ring-breathing vibration and the overtone of an out-of-plane ring-bending vibration of tyrosyl residues (847 and 835 cm^{-1}). These Raman bands indicate that the microcolony is protein-rich. The dominant constituent of the biofilm structure is known to be exopolysaccharides, so the remaining Raman bands may be assigned to polysaccharide vibrations. In particular, colanic acid,[36] which is the exopolysaccharide produced by a mucoid *E. coli* strain, is one of the most plausible candidates. A previous study using microanalytical methods[37] show that the composition of colanic acid produced by *E. coli* S53 strain is: fucose, 30.4%; glucose, 18.2%; galactose, 26.0%; and glucuronic acid, 18.0%. We are currently measuring reference Raman spectra of those compounds in order to compare with spectrum A (or B) in Fig.10.

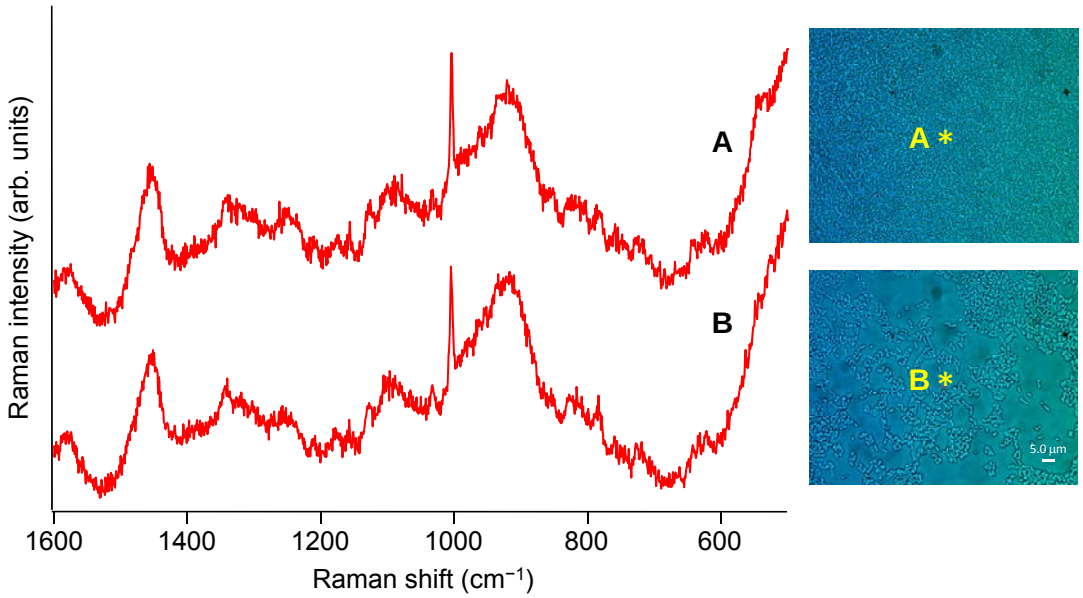

Fig. 9. Space-resolved Raman spectra of a biofilm that consists of *E. coli* measured 24 hours after starting cell culture. The laser power at the sample was 5 mW, and the accumulation time was 100 s.

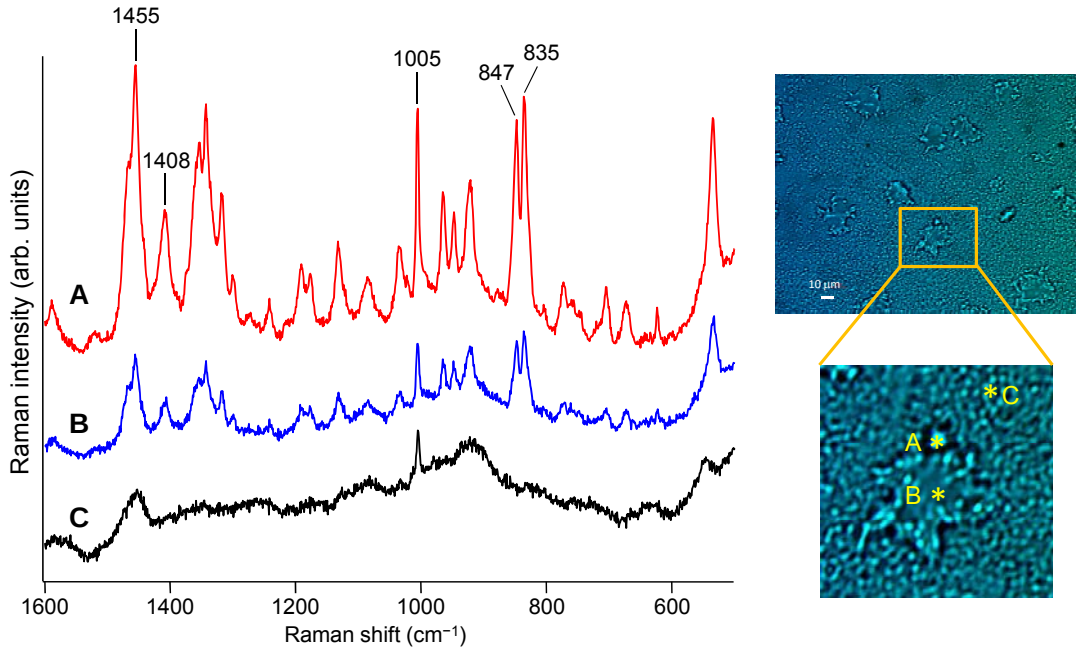

Fig. 10. Space-resolved Raman spectra of the *E. coli* biofilm measured one week after starting cell culture. The laser power at the sample was 5 mW, and the accumulation time was 60 s.

To reveal molecular distribution inside the microcolony, we did a Raman mapping experiment.[38,39] In the Raman mapping experiment, the sample is scanned by using the piezoelectric stage with the laser focus fixed, and the Raman spectrum is recorded at each point on the sample. Subsequently the two-dimensional map of the intensity distribution of

each band is constructed via curve fitting or spectral integration. Raman images obtained from a microcolony in the one-week *E. coli* biofilm are displayed in Fig. 11 for the bands at 1455, 1408, 1004, 922, 833, and 533 cm^{-1}, together with an optical micrograph of the microcolony. The dimension of each image is 15 × 16 μm. The Raman images in Fig. 11 clearly visualize highly heterogenous nature of the biofilm. It follows from the images that molecular species responsible for the six Raman bands are well localized in the microcolony, and that they show quite similar distributions.

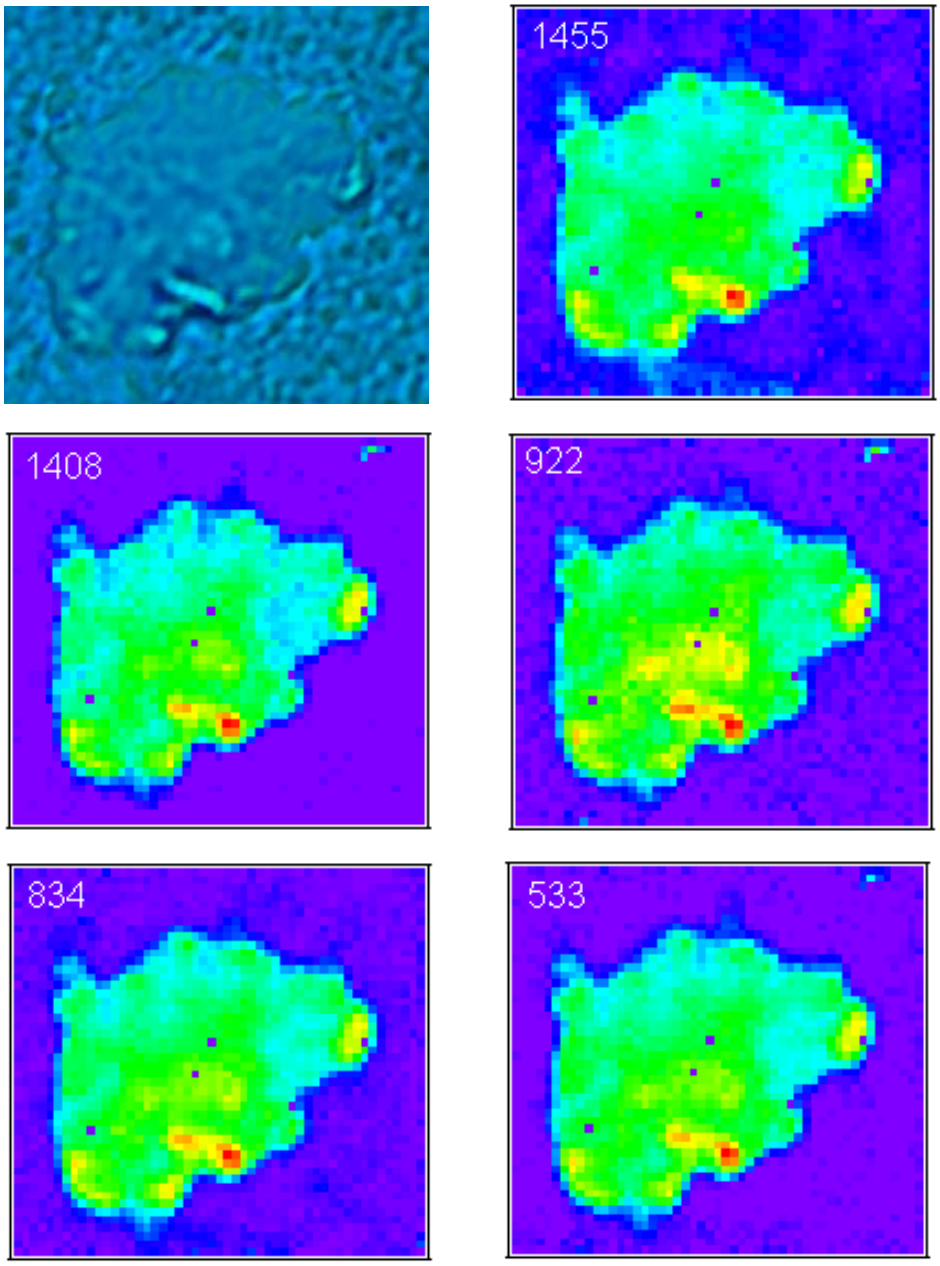

Fig. 11. Raman mapping result of a microcolony of the 24-h *E.coli* biofilm. The left image in the top row represents an optical micrograph of the colony, and the others are Raman images for the bands at 1455, 1408, 922, 834, and 533 cm^{-1}. Red color corresponds to higher intensities, while blue lower.

4. References

1. X. D. Zhu, H. Shur, and Y. R. Shen, *Phys. Rev. Lett.* **35**, 3047 (1987).
2. S. Mukamel, *Principles of Nonlinear Optical Spectroscopy*, Oxford Press, New York, 1995.
3. Y. R. Shen, *The Principles of Nonlinear Optics*, Wiley, New York, 1984.
4. P. B. Miranda and Y. R. Shen, *J. Phys. Chem B* **103**, 3292 (1999).
5. T. Iimori, T. Iwahashi, H. Ishii, K. Seki, Y. Ouchi, R. Ozawa, H. Hamaguchi, and D. Kim, *Chem. Phys. Lett.* **389**, 321 (2004).
6. C. D. Bain, *J. Chem. Soc. Faraday Trans.* **91**, 1281 (1995).
7. T. Ishibashi, M. Ara, H. Tada, and H. Onishi, *Chem. Phys. Lett.* **367**, 376 (2003).
8. C. Weeraman, A. K. Yatawara, A. N. Bordenyuk, and A. V. Benderskii, *J. Am. Chem. Soc.* **128**, 14244 (2006).
9. G. A. Somorjai and G. Rupprechter, *J. Phys. Chem. B* **103**, 1623 (1999).
10. R. D. Schaller, J. C. Johnson, K. R. Wilson, L. F. Lee, L. H. Harber, and R. J. Saykally, *J. Phys. Chem. B* **106**, 5143 (2002).
11. Y. Shen, J. Swiatkiewicz, J. Winiarz, P. Markowicz, and P. N. Prasad, *Appl. Phys. Lett.* **77**, 2946 (2000).
12. D. M. P. Hoffmann, K. Kuhnke, and K. Kern, *Rev. Sci. Instrum.* **73**, 3221 (2002).
13. G. Mizutani, T. Koyama, S. Tomizawa, and H. Sano, *Spectrochim. Acta A* **62**, 845 (2005).
14. K. Cimatu and S. Baldelli, *J. Phys. Chem. B* **110**, 1807 (2006).
15. A. L. Harris, L. Rothberg, L. Dhar, N. J. Levinos, and L. H. Dubois, *J. Chem. Phys.* **94**, 2438 (1991).
16. C. Hirose, A. Bandara, S. Katano, J. Kubota, A. Wada, and K. Domen, *Appl. Phys. B* **68**, 559 (1999).
17. E. H. G. Backus, A. Eichler, A. W. Kleyn, and M. Bonn, *Science*, **310**, 1790 (2005).
18. J. A. McGuire and Y. R. Shen, *Science*, **313**, 1945 (2006).
19. R. M. Donlan and J. W. Costerton, *Clin. Microbiol. Rev.* **15**, 167 (2002).
20. D. Davis, *Nat. Rev. Drug Discov.* **2**, 114 (2003).
21. J. W. Costerton, Z. Lewandowski, D. E. Caldwell, D. R. Korber, and H. M. Lappin-Scott, *Annu. Rev. Microbiol.* **49**, 711 (1995).
22. W. C. Fuqua, S. C. Winans, and E. P. Greenberg, *J. Bacteriol.* **176**, 269 (1994).
23. R. Pätzold, M. Keuntje, and A. Anderson-von Ahlften, *Anal. Bioanal. Chem.* **386**, 286 (2006).
24. C. Sandt, T. Smith Palmer, J. Pink, and D. Pink, *J. Microbiol. Methods*, **75**, 148 (2008).
25. N. P. Ivleva, M. Wagner, H. Horn, R. Niessner, and C. Haisch, *Anal. Bioanal. Chem.* **393**,

197 (2009).
26. N. P. Ivleva, M. Wagner, H. Horn, R. Niessner, and C. Haisch, *Anal. Chem.* **80**, 8538 (2008).
27. H.-Y. N. Horman, R. Miles, Z. Hao, E. Wozei, L. M. Anderson, and H. Yang, *Anal. Chem.* **81**, 8564 (2009).
28. L.-P. Choo-Smith, K. Maquelin, T. Van Vreeswijk, H. A. Bruining, G. J. Puppels, N. A. Ngo Thi, C. Kirschner, D. Naumann, D. Ami, A. M. Villa, F. Orsini, S. M. Doglia, H. Lamfarraj, G. D. Sockalingum, M. Manfait, P. Allouch, and H. P. Endtz, *Appl. Environ. Microbiol.* **67**, 1461 (2001).
29. T. Ishibashi and H. Onishi, *Appl. Phys. Lett.* **81**, 1338 (2002).
30. J. A. Carter, Z. Wang, and D. D. Dlott, *Acc. Chem. Res.* **42**, 1343 (2009).
31. P. R. Carey, *Biochemical Applications of Raman and Resonance Raman Spectroscopies*, Academic Press, New York, 1982.
32. J. De Gelder, K. De Gussem, P. Vandenabeele, and L. Moens, *J. Raman. Spectrosc.* **38**, 1133 (2007).
33. M. Wagner, N. P. Ivleva, C. Haisch, R. Niessner, and H. Horn, *Water Res.* **43**, 63 (2009).
34. C. Xie and Y.-Q. Li, *J. Appl. Phys.* **93**, 2982 (2003).
35. M. N. Siamwiza, R. C. Lord, M. C. Chen, T. Takamatsu, I. Harada, H. Matsuura, T. Shimanouchi, *Biochemistry*, **14**, 4870 (1975).
36. W. F. Goebel, *Proc. Natl. Acad. Sci. USA*, **49**, 464 (1963).
37. I. W. Sutherland, *Biochem. J.* **115**, 935 (1969).
38. Y.-S. Huang, T. Karashima, M. Yamamoto, and H. Hamaguchi, *Biochemistry*, **44**, 10009 (2005).
39. Y. Naito, A. Toh-e, and H. Hamaguchi, *J. Raman Spectrosc.* **36**, 837 (2005).

5. Self-evaluation

Due mainly to the delay in construction of University facilities and many troubles in the laser, unfortunately the outcomes reported here are a bit different from what was anticipated. We deeply regret that the development of the SFG imaging microscope system has not been completed within the term of execution. As reported above, we are done with the construction of the sample part and laser training for a student involved. We also took advantage of the CCD camera that we purchased for the project and implemented it in a Raman microscope system so as not to waste this expensive instrument. With this, it has become possible to carry out molecular vibrational imaging of biologically relevant surfaces, which is one of the goals of this project, although the use of Raman microspectroscopy was not included in the

proposal. To the best of our knowledge, our study of the *E. coli* biofilm is the first to show comprehensive *in situ* analysis of biofilms. There indeed are several reports on Raman studies of biofilms, but none of them chemically identifies exopolysaccharides produced in the biofilms they studied and clarify the structure–function interplay. We will publish the results in a high-impact factor journal as soon as we are done with the assignment of the observed Raman bands. Our detailed study will bring about a broad impact in a variety of fields including microbiology, ecology, and medicine. For instance, if the EPS composition of a biofilm is determined by this method, then it will be possible to predict reagents that can efficiently remove the EPS from the surface to which the biofilm adheres. Such an efficient removal of EPS will be of great help for reducing bacterial infections of medical instruments. Finally, needless to add, we are continuously making every effort to finish developing the SFG imaging microscope.

6. Appendix

The poster presented in the conference “Annual Meeting of Japan Society for Molecular Science”.

活性汚泥中のバイオフィルムの顕微ラマン分析

(National Chiao Tung Univ.[1], 筑波大院生命環境科学[2], 東大院理[3])
○重藤真介[1], Hemanth Nag[1], 八幡穣[2], 野村暢彦[2], 濵口宏夫[1,3]

Introduction—What are biofilms?

● バイオフィルムとは

多糖類などの細胞外高分子物質(extra-cellular polymeric substances, EPS)のマトリックス中に形成される，バクテリアや菌類の凝集体。

- カテーテルやコンタクトレンズなどの医療用器具から，パイプや石の表面に至るまで，多様な環境に形成される。
- 抗菌剤への耐性，内部環境の恒常性保持。
- EPSを通じた物質輸送，バクテリア同士の情報伝達

単一細胞レベルで，バイオフィルムの構造と機能の関係を明らかにすることが重要

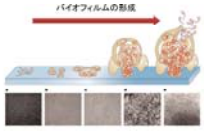

Nat. Rev. Drug. Discov. 2, 114 (2003)

● 顕微ラマン分光法

- Sub-μmの空間分解能での非破壊・非侵襲分析が可能。
- 生物試料でしばしば問題となる水の妨害を受けにくい。
- 染色などの前処理が必要なく，探索的な研究が可能。
- 振動スペクトルを通じて，測定対象中の分子種に固有な情報が得られる。

● 本研究の目的

- 廃水処理施設で実際に用いられている活性汚泥中のバイオフィルムに，どのような物質が，どのような形態で存在しているのかを分子レベルで研究。
- バイオフィルムが示す機能と構造との関わりを，顕微ラマン分光法を用いて*in situ*に研究するための足がかりを得る。

Experimental

● 実験装置：共焦点顕微ラマン分光計

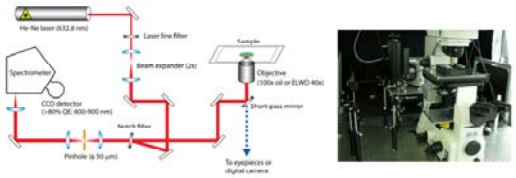

- 空間分解能：XY ~300 nm, Z ~4 μm
- 指紋領域からCH伸縮振動領域までのラマンスペクトルを測定可能。
- XYZ3軸ピエゾステージによる3次元マッピング（最大 300 μm × 300 μm × 300 μm ）。

測定例

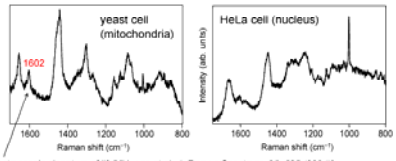

"Raman spectroscopic signature of life" [Huang et al. J. Raman Spectroac. 35, 525 (2004)]

● 試料：活性汚泥中のバイオフィルム

活性汚泥中のバイオフィルム2種（1および2）
1：白色不透明のフィルム状
2：暗緑色の懸濁液

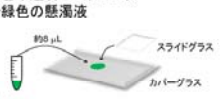

測定条件
試料位置におけるレーザーパワー：1.2 mW
露光時間：60秒（バイオフィルム1），10秒（バイオフィルム2）

Results: Biofilm 1

● スペクトル①

- 1514 cm^{-1}: C=C伸縮振動
- 1159 cm^{-1}: C–C伸縮振動
- 1010 cm^{-1}: CH_3横ゆれ

カロテノイドの凝集体の存在を示唆

その他の微弱なラマンバンドの振動数も代表的なカロテノイドのものとほぼ一致。

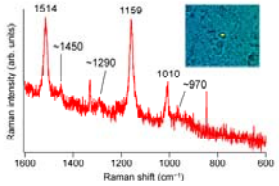

● スペクトル②

小胞状構造内に存在する黒い球状の物体(A)のラマンスペクトル

- 炭素骨格に特徴的なラマンバンド（CH変角など）が強く観測されていない。
- 非常に強いバンドの振動数 996 cm^{-1} ~ SO_4^{2-}の対称伸縮の振動数

Gypsumのような硫酸塩を主成分とした鉱物

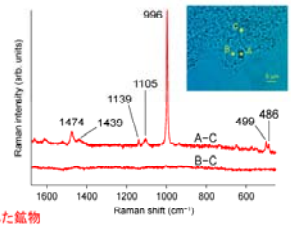

Results: Biofilm 2

バイオフィルム2中には、光学像およびSEM像が示すような「らせん構造」が多く見られる。

- Spirulina (*Arthrospira platensis*)

単細胞藻類の一種。
主な構成成分は，タンパク質，カロテノイド，多糖類，クロロフィルなど。

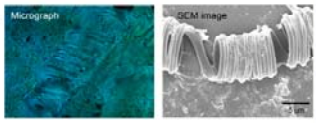

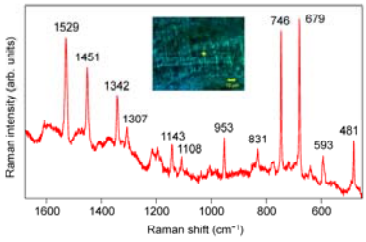

タンパク質：~1660 cm^{-1}（アミドI），~1450cm^{-1}（CH変角），~1250 cm^{-1}（アミドIII），~1000 cm^{-1}（フェニルアラニン残基）
多糖類：1650–1540 cm^{-1}（COO^-逆対称伸縮），1450–1360 cm^{-1}（COO^-対称伸縮），~1125/1090/890 cm^{-1}（グリコシド結合），480–300 cm^{-1}

Refs) P. R. Carey, "Biochemical Applications of Raman and Resonance Raman Spectroscopies", Academic Press
N. P. Ivleva, N. Wagner, H. Horn, R. Niessner, C. Haisch, Anal. Bioanal. Chem. 393, 187 (2009).

Future work

● Quorum sensing

バクテリアが生育環境の細菌密度を感知して，物質産生を制御する機構。

どのような物質がオートインデューサーとして働き，どのように情報がバイオフィルムのコロニー間を伝達されるのか？

➡ 顕微ラマン分光法による研究

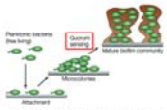

Nat. Rev. Mol. Cell Biol. 3, 685 (2002)

Financial support: Ministry of Education (MOE-ATU plan) and National Science Council under contract NSC 97-2113-M-009-002-MY2

Stating that this paper is based on work sponsored by NSC.